



Mechanical behaviour and corrosion study of 304L austenitic steel processed by constrained groove pressing

Rahul Singh, Samarjit Singh, Balina Kranthi Kumar & Abhishek Kumar*

Department of Applied Mechanics, Motilal Nehru National Institute of Technology Allahabad, Prayagraj 211 004, India

Received: 30 January 2021; Accepted: 06 June 2021

In the present work, 304L-austenitic stainless steel has been successfully processed till two passes of constrained groove pressing (CGP). The processed steel has been characterized using X-ray diffraction and a vibrating sample magnetometer. The XRD patterns and vibrating sample magnetometer confirms phase transformation (austenitic phase to martensitic phase). CGP of 304L austenitic steel improves mechanical properties such as tensile strength, yield strength and micro-hardness. The ultimate tensile strength value improves from 775 MPa to 1156 MPa, the value of yield strength improves from 332 MPa to 639 MPa and the microhardness improves from 244 VHN to 476 VHN for solution-treated, and two pass CGP processed specimens, respectively. The influence of CGP has also been reflected in electron backscatter diffraction (EBSD) results in terms of more substructure formation. The corrosion behavior has been estimated via linear polarization and electrochemical impedance spectroscopy tests. The CGPed 304L steel shows poor resistance to corrosion in comparison to parent steel. Polarization resistance values decrease from 27.88 to 12.63 $k\Omega/cm^2$ which represents loose and less protective passivating film after CGP.

Keywords: Austenitic stainless steel (Type-304L), Constrained groove pressing, Corrosion behavior, Phase transformation

1 Introduction

Over the past couple of decades, numerous severe plastic deformation techniques are developed and proposed. Severe Plastic Deformation (SPD) techniques are metal forming processes/routes, where a huge amount of plastic strain is imposed to produce ultra-fine grain materials. Shin¹ in the year 2002, introduced a new SPD technique based on repetitive corrugating and straightening for the pure aluminum sheet, which is named constrained groove pressing (CGP). Thereafter, CGP has been applied over a variety of metals and alloys. Pure aluminum, aluminum alloys, pure copper, copper-based alloys, pure nickel, and low carbon steels have been successfully processed via CGP for obtaining fine-grained materials².

Austenitic stainless steels are among the important stainless-steel family used in a wide range of industrial sectors³. Numerous industrial applications are mainly attributed to their outstanding resistance to corrosion (oxidation), and their ability to form thin sheets (superior malleability). However, their moderate strength (due to soft face-centered cubic austenite

phase (γ)) limits their technological applications range^{3,4}. Improvement in the strength of stainless steels can be achieved by alteration in structural grain size (grain refinement), work hardening, and solid solution strengthening⁵⁻⁷. A lot of research has been carried out in the last decades on the CGP of different materials. However, there is a need to systematically study the deformation behavior of 304L austenitic stainless steel employing CGP. Therefore, in this present research work, an effort has been made to explore the effect of CGP on microstructure, mechanical behavior, phase transformation, and corrosion nature of 304L austenitic steel.

2 Materials and Methods

In this study, the commercially available 304L austenitic steel has been purchased from the local market. The elemental composition of the steel is given in Table 1. Specimens of the cross-sectional area of 60 mm \times 50 mm \times 3 mm were sectioned and solution-treated at 1050 °C before processing. Fig. 1 shows different stages of a single CGP pass. A single pass of CGP consists of four stages viz. grooving followed by flattening and then 180° rotation of specimen followed by steps of grooving and flattening. After completion of one pass, the strain

*Corresponding author (E-mail: abhishek@mnnit.ac.in)

Table 1 — Elemental composition of 304L austenitic stainless steel (Weight %) used in present research work

Element	C	Ni	Cr	Mo	Mn	P	Si	S	Fe
Content wt%	0.03	8.094	18.22	0.14	1.70	0.035	0.191	0.007	Balance

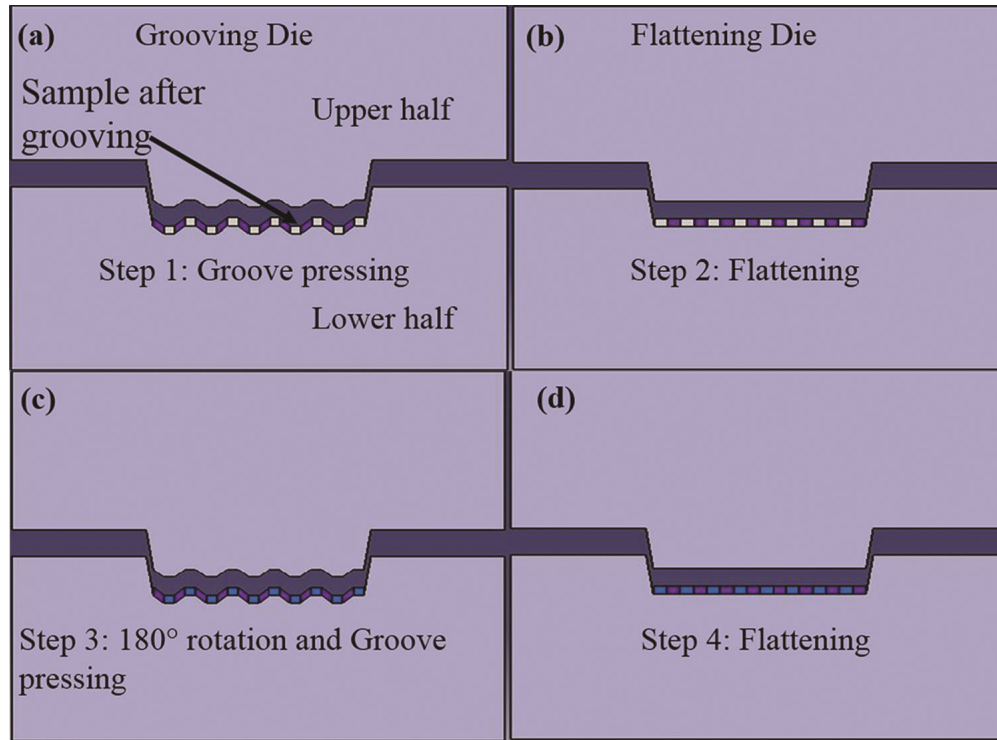


Fig. 1 — Schematic representation of the constrained groove pressing.

of 1.16 is induced uniformly throughout the specimen.

X-ray diffraction (XRD) and vibrating sample magnetometer (VSM) studies were performed to investigate phase transformation in CGPed specimens. XRD studies were conducted employing Rigaku Smartlab diffractometer. Light optical microscopy (LOM) using Leica 5000M was employed for the micrographs. Electron backscatter diffraction (EBSD) measurements were conducted on small coupons of size 10 mm × 10 mm. FEI-Nova machine was used to perform the EBSD measurements. The measured data of EBSD was analyzed using TSL OIM software. The effect of CGP on mechanical properties was investigated via tensile and hardness tests. Tensile samples of the different CGPed steel were fabricated in accordance with ASTM E8 with a gauge length of 16 mm. Tensile tests were performed at room temperature on a BISS tensile testing machine of load cell 25 kN with constant crosshead movement of 0.05 mm/min. A minimum of five tests were conducted for each condition. Microhardness tests employing UHL-

VMHT machine were conducted to record Vickers hardness values at room temperature, taking a load of 500 gf for 15 seconds dwell time. The indents were made along a straight line at various points evenly spaced over the surface. Corrosion behavior of CGPed steel specimens was inspected *via* electrochemical impedance spectroscopy (EIS) and polarization tests employing AUTOLAB potentiostat-galvanostat. NOVA software was used to analyze the output of the corrosion tests. A three-electrode cell was used to conduct all corrosion tests at room temperature with an exposed area of 1 cm². Ag/AgCl reference electrode, platinum mesh as a counter electrode and processed steel (with varied thickness reductions) as a working electrode were used to perform corrosion tests in 3.5% NaCl solution as an electrolyte.

3 Results and Discussion

This section emphasizes the phase, morphological, magnetic, EBSD, mechanical, and corrosion analysis of the CGPed steel specimens.

3.1 X-ray diffraction analysis

XRD patterns of 304L steel samples undergone two passes of constrained groove pressing are shown in Fig. 2. The un-deformed stainless steel (0 Pass condition) sample indicates the presence of peaks corresponding to planes (111), (200), (220), and (311) in the austenite phase. The new peaks of α' -martensite phase (deformation-induced martensite) appear with progress in CGP passes and the austenitic phase γ starts disappearing. The martensitic peaks indexed with planes of reflections (110) and (211) start emerging, indicating the growth of martensitic phase with CGP.

3.2 Magnetic measurements

XRD results of 304L austenitic steel undergone CGP have both austenitic and martensitic phases. The amount of phase conversion (austenitic to martensitic) depends on the amount of strain developed during CGP passes. The martensitic transformation can be identified using magnetization curves obtained as a result of the VSM tests. The austenite phase is non-ferromagnetic at ambient conditions (room temperature), *i.e.*, it shows nearly zero saturation magnetization; while on the contrary α' -martensite is ferromagnetic³. The volume fractions of α' -martensite can be obtained using saturation magnetization⁸. Therefore, saturation magnetization values from VSM characterization (as shown in Fig. 3) were used to calculate the volume fraction of α' -martensite. Table 2 shows the volume fraction of austenite and α' -martensite as a function CGP passes. The trend of volume fraction shows a monotonic increase with the progress in CGP passes reflecting more ferromagnetic characteristics.

3.3 EBSD analysis

The deformation mechanism in steels strongly depends on stacking fault energy (SFE), and it can be calculated from the chemical composition of steel.

$$\text{Stacking fault energy (SFE)} \left(\frac{\text{mJ}}{\text{m}^2} \right) = -53 + 6.2(\%Ni) + 0.7(\%Cr) + 3.2(\%Mn)9.3(\%Mo) \quad \dots (1)$$

Putting the chemical composition of steel in Eq. (1), the SFE of 304L austenitic steel is estimated to be 16.74 mJ/m². Two major paths for the martensitic transformation of austenitic steels were proposed by Olsen *et al.*⁹ and Sato *et al.*¹⁰.

(i) Austenite (γ) \rightarrow martensite (ϵ) \rightarrow α' -martensite (SFE < 18 mJ/m²), and

(ii) Austenite (γ) \rightarrow twinned austenite \rightarrow α' -martensite (SFE > 18 mJ/m²).

As per SFE, phase transformation in 304L steel should follow path 1. Deformation-induced martensite regions are the areas of large strain gradients such as vicinities of grain boundaries and microshear bands. Figure 4 shows the optical micrograph of the solution-

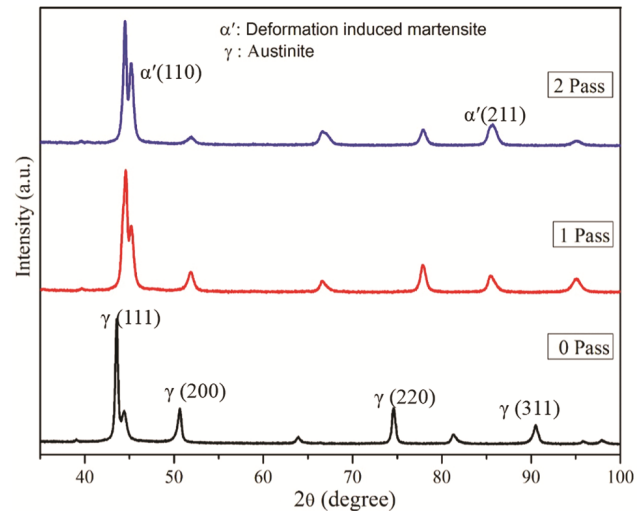


Fig. 2 — The XRD patterns of CGPed 304L austenitic stainless steel.

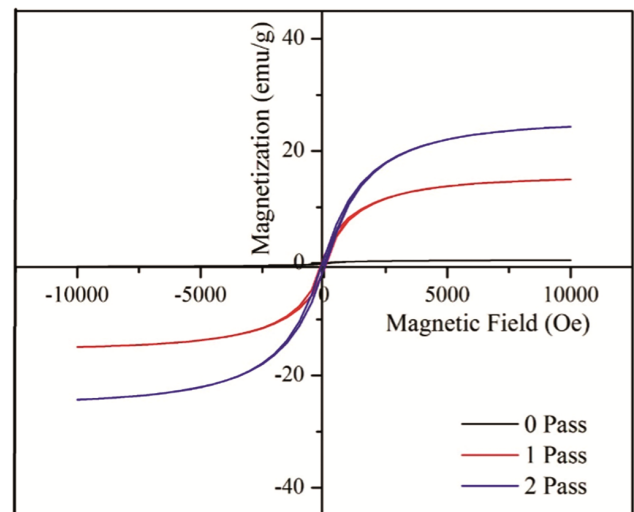


Fig. 3 — Hysteresis curves of CGPed austenitic stainless steel.

Table 2 — Amount of the martensite and austenite phases in CGPed 304L austenitic stainless steel obtained *via* VSM

Sample condition	Saturation magnetization (emu/g)	% volume fraction austenite	% volume fraction α' -martensite
0 Pass	0.559	0.99	0.003
1 Pass	14.93	0.90	0.096
2 Pass	24.34	0.84	0.158

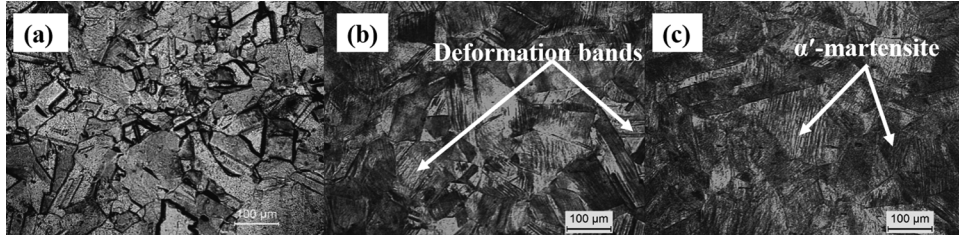


Fig. 4 — Optical micrograph of (a) solution treated, (b) 1 pass, and (c) 2 pass conditioned steel.

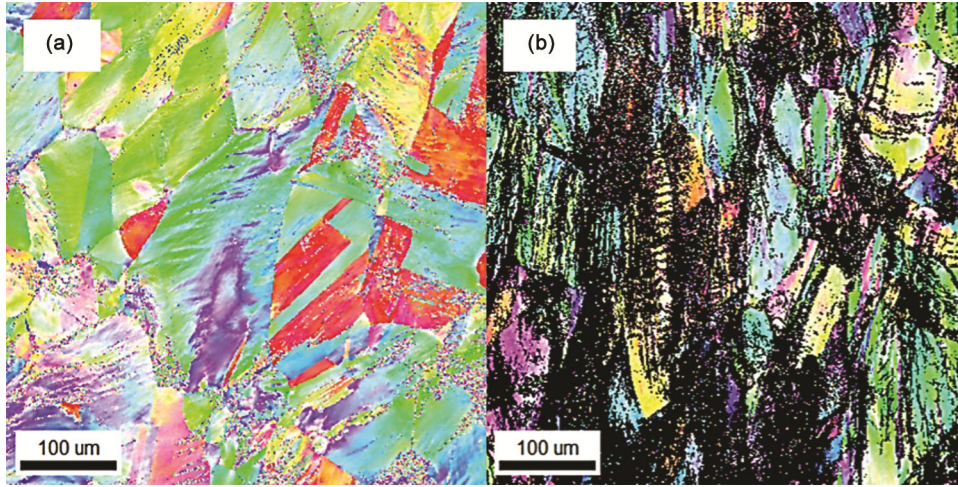


Fig. 5 — IPF of CGPed 304L austenitic stainless steel (a) after 1 pass, and (b) after pass 2.

treated and CGPed steel. Solution-treated specimen (Fig. 4(a)), which on deformation (1 pass) results in the generation of shear/deformation bands (Fig. 4(b)), and these shear bands transform to α' -martensite¹¹ as visible in Fig. 4(c). To understand evolution of substructure during CGP, EBSD measurements were performed. The EBSD images, as shown in Fig. 5, represent inverse pole figure (IPF) maps of steel obtained after pass 1 (Fig. 5(a)) and pass 2 (Fig. 5(b)). During CGP, substructure formation occurs, and subgrains are developed represented by the gradient of color within the grain. Figure 6 depicts the distribution of misorientation angle obtained from EBSD. In solution-treated (0 pass) specimen, a large amount of high angle grain boundaries (HAGBs) are observed. As the 304L steel undergo CGP, the plastic deformation influences the development of substructures, and more subgrain boundaries are formed. The extent of subgrain formation is marginally high for the pass 2 specimen, which is reflected as the increase in low angle grain boundaries (LAGBs) fractions having misorientation less than 10° . Figure 7 shows grain size variation with CGP and resulted in the refinement of steel grains. The austenitic grain size reduces from $10\ \mu\text{m}$ to $1\ \mu\text{m}$ after two passes of CGP.

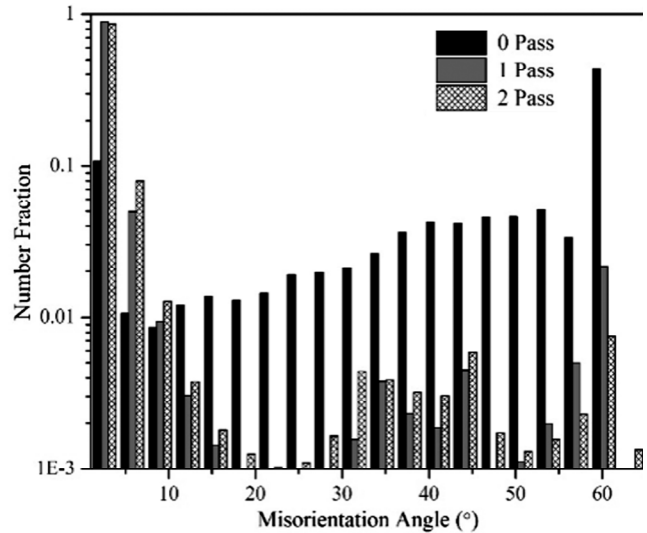


Fig. 6 — Histograms of misorientation angle of solution-treated and CGPed specimens.

3.4 Mechanical characterization

The engineering stress-strain curve of 304L austenitic steel obtained after two passes of CGP are shown in Fig. 8. The curve shows CGP improves the yield strength as well as ultimate tensile strength (UTS) of the steel, however, the ductility of steel decreases with CGP. Figure 9 shows the effect of

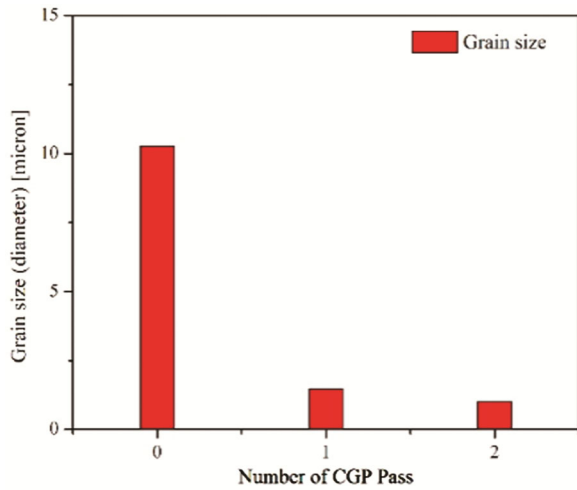


Fig. 7 — Grain size variation with CGP obtained from EBSD analysis.

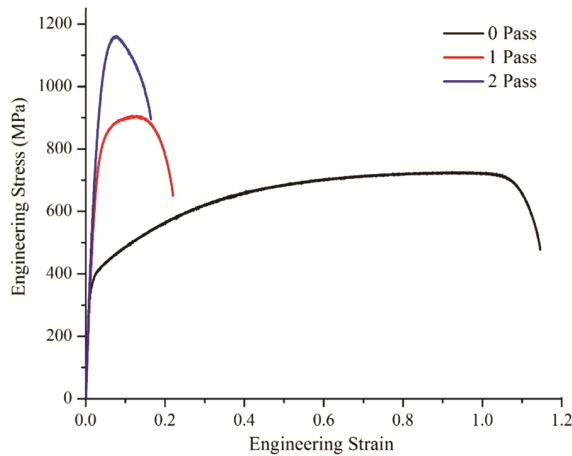


Fig. 8 — Engineering stress- strain curve of 304L austenitic steel after 0, 1 and 2 Pass of CGP.

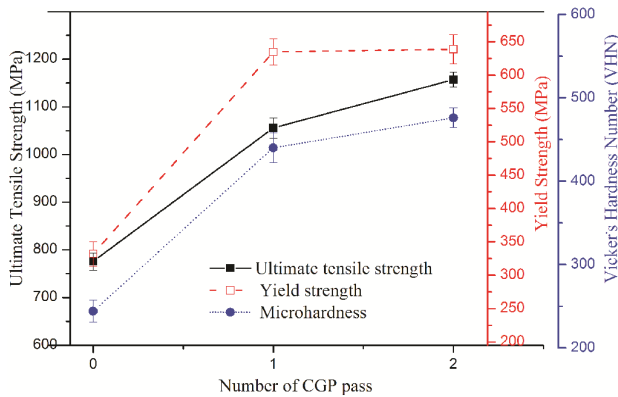


Fig. 9 — Improvement in microhardness, yield strength and ultimate tensile strength with CGP passes.

CGP on the mechanical properties. The UTS of solution-treated steel (*i.e.*, 0 Pass) is improved from 755 MPa to 1156 MPa after two passes. The yield

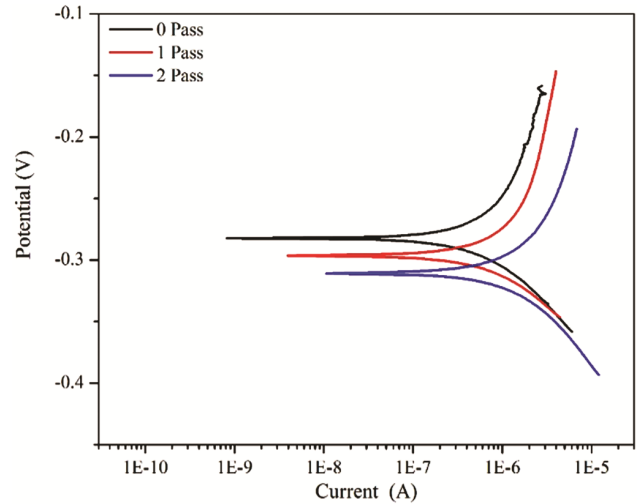


Fig. 10 — Linear polarization plots of CGPed austenitic steel.

strength enhances from 332 MPa to 639 MPa after two passes of CGP. The average hardness value of solution-treated steel improves with CGP. The hardness values have increased from 244 VHN to 476 VHN after the completion of two CGP passes.

3.5 Corrosion study

Figure 10 shows the linear polarization curves for the solution-treated and CGPed samples in the 3.5% NaCl solution. All electrochemical corrosion parameters acquired from the polarization curves are tabulated in Table 3. According to obtained results, I_{corr} (corrosion current) increases sharply from $1.24E-06$ for 0 pass to $3.8E-06$ after two passes of CGP. The polarization resistance R_p decreases from $27.88 \text{ k}\Omega/\text{cm}^2$ to $12.63 \text{ k}\Omega/\text{cm}^2$ after two passes of CGP. Therefore, the corrosion rate increases with an increase in CGP passes. A decrease in corrosion resistance occurs mainly because of an increased level of lattice defects *i.e.* higher dislocation density and higher low angle grain boundaries. The atoms seated at these locations go into the solution as a result of their less stable crystalline domain. As the rate of corrosion reaction is directly proportional to the concentration of reactive spots, the concentration of lattice defects increases, the corrosion rate is increased¹². In addition, corrosion rate is also in direct relation to the amount of α' -martensite, which in turn, is directly proportional to the degree of deformation¹². Electrochemical impedance spectroscopy tests were conducted to study the effect of CGP on passive film resistance of the 304L austenitic steel. Figure 11 depicts Nyquist plot (Fig. 11(a)) and Bode phase formalism (Fig. 11(b)) for solution-treated and CGPed

Table 3 — The corrosion parameters from polarization test

Specimen condition	OCP	E_{corr} (V)	Ba (V/dec)	Bc (V/dec)	I_{corr} (A)	Corrosion rate (mm/Yr)	Polarization resistance ($\text{k}\Omega/\text{cm}^2$)
0 Pass	-0.259	-0.2823	0.10542	0.32773	1.24E-06	0.014435	27.88
1 Pass	-0.248	-0.2964	0.09825	0.28481	1.66E-06	0.019233	19.17
2 Pass	-0.294	-0.3108	0.14769	0.44129	3.80E-06	0.044186	12.63

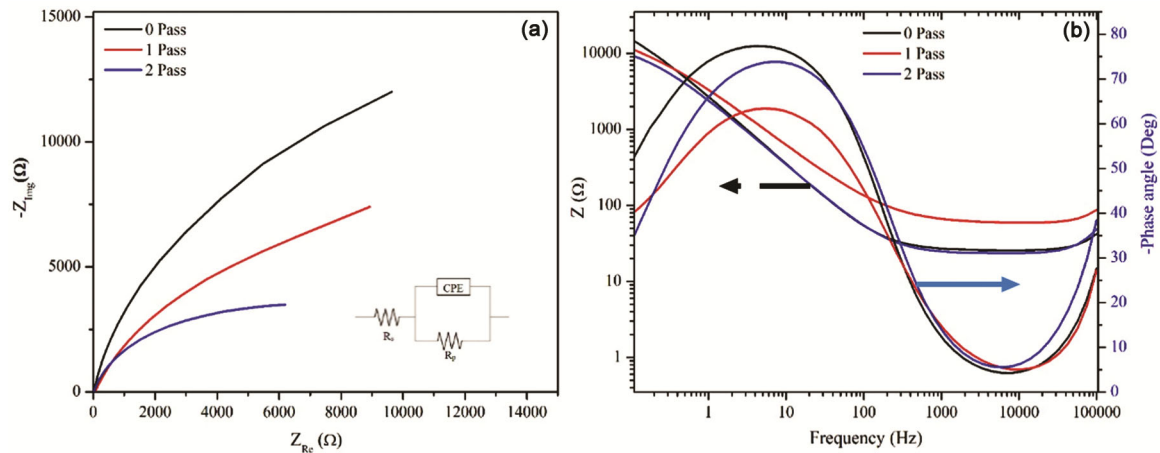


Fig. 11 — (a) Nyquist plot of CGPed steel, and (b) representing corresponding bode plot.

Table 4 —The corrosion parameters from EIS test.

Specimen condition	R_s (Ω)	R_p ($\text{k}\Omega$)	CPE	
			Y_0 (μmho)	N
0 Pass	26.2	28.8	71.9	0.893
1 Pass	59.2	19.4	71.4	0.761
2 Pass	23.7	12.4	80.2	0.871

samples. Nova 1.8 software was used to fit each spectra as per the equivalent circuit model, as illustrated in Fig. 11(a).

Equivalent electrical parameters obtained are tabulated in Table 4, where, R_s refers to solution resistance between specimen and reference electrode, R_p implies charge-transfer resistance (polarization resistance) of all electrode reactions of the system, and CPE is constant phase element. Nyquist plots are unfinished semicircle¹². The more the diameter of the semicircle, better the resistance of the film, which affirms with increasing strain, the resistances of the film deplete¹². In bode plots, at low frequency, the adverse effect of CGP is mirrored as low frequency phase angle reduce with increase in CGP passes, showing indications of defective film. R_s values are in between 26–59 Ω , however; R_p decreases with an increase in CGP passes (Table 4). The decrease in R_p indicates increased electrochemical reactions at film, and it may also indicate that passivating film resistance decrease with increasing CGP pass. Low

values of capacitance refer to a thick film and vice-versa¹³. The increase in CPE value with progressing CGP passes indicates less resistant passivating film. Moreover, film resistance is inversely proportional to defect densities¹³ *i.e.*, high defect densities will result in loose and less protective passivating film, with lower R_p .

4 Conclusion

In the present study, 304L austenitic stainless steel has been successfully constrained groove pressed for two passes. CGP of 304L austenitic steel results in improvement in mechanical properties like tensile strength, yield strength, and microhardness. The ultimate tensile strength, yield strength and microhardness values improve from 775 MPa to 1156 MPa; from 332 MPa to 639 MPa and from 244 VHN to 476 VHN after two passes of CGP, respectively. Ductility experiences a significant reduction in their magnitudes with the increase in the number of CGP passes. Austenitic to martensitic phase transformation is encountered and increase swiftly with the increased strain *i.e.*, with increasing CGP passes. CGP of 304L steel results in grain refinement and shows inferior resistance to corrosion.

Acknowledgment

The authors are thankful to the Centre of Interdisciplinary Research Laboratory, MNNIT

Allahabad, Prayagraj and National facility IIT Bombay for providing the characterization facilities. The first two authors would like to thank the Ministry of Human Resource and Development, India, for his fellowship.

References

- 1 Shin D H, Park J J, Kim Y S, & Park K T, *Mater Sci Eng A*, 328 (2002) 98.
- 2 Gupta A K, Maddukuri T S, & Singh S K, *Prog Mater Sci*, 84 (2016) 403.
- 3 Tanhaei S, Gheisari Kh, & Alavi Zaree S R, *Int J Miner Metall*, 25 (2018) 630.
- 4 Singh R, Goel S, Verma R, Jayaganthan R, & Kumar A, *IOP Con Ser: Mater Sci Eng*, 330 (2018) 012017.
- 5 Singh R, Yadav S D, Malviya N, Goel S, Jayaganthan R, & Kumar A, *Mater Sci Forum*, 969 (2019) 508.
- 6 Singh R, Sachan D, Goel S, Verma R, Jayaganthan R, & Kumar A, *Mater Today: Proc*, 5 (2018) 16880.
- 7 Singh R, Rajan G, Kumar B K, Verma R, Singh D, Rao P N, Jayaganthan R, & Kumar A, *Mater Sci Forum*, 969 (2019) 901.
- 8 Singh R, Singh D, Sachan D, Yadav S D, & Kumar A, *J Mater Eng Perform*, 30 (2021) 290.
- 9 Olsen G B, & Cohen M, *Metall Trans A*, 6 (1975) 791.
- 10 Sato K, Ichinose M, Ohirotso Y, & Inoue Y, *ISIJ Int*, 29 (1989) 868.
- 11 Hadji M, & Badji R, *J Mater Eng Perform*, 11 (2002) 145.
- 12 Tandon V, Patil A P, Rathod R C, & Shukla S, *Mater Res Express*, 5 (2018) 026528.
- 13 Kurc A, Kciuk M, & Basiaga M, *J Achiev Mater Manuf Eng*, 38 (2010) 154.